An Efficient Insertion Control Method for Precision Assembly of Cylindrical Components

Song Liu, You-Fu Li, *Senior Member, IEEE*, Deng-Peng Xing, De Xu, *Senior Member, IEEE*, and Hu Su

***Abstract*—In this paper, an efficient insertion control strategy is presented for precision assembly of cylindrical components with interference fit. It has two inherent advantages compared with existing insertion methods in the domain of precision assembly. First, it does not need preparatory actions dedicated for horizontal forces before insertion actions, which is realized by integrating the preparations into the insertion step. Second, instead of inserting with fixed incremental depth, it estimates the insertion depth for every action to be as large as possible with a probabilistic approach. Specifically, the insertion of components is modeled as a stochastic state transition process with the uncertainty described by Gaussian distribution. The state transition function is well defined based on analysis of the historical assembly data and the universal mechanical properties of the components. An assessment function is also elaborately designed to evaluate the performance of the state transition function in order to stimulate the control strategy to behave progressively or conservatively. Finally, the action to be taken for the current state is decided by iterative calculations in *N* steps estimation manner. An automatic assembly system is developed to verify the effectiveness of the proposed control method. Experimental results show that the assembly process with the proposed insertion control strategy can finish within 30 steps, which is at least four times more efficient than the process with the traditional method.**

***Index Terms*—Assessment function, discount factor, insertion control strategy, insertion depth estimation, precision assembly, stochastic state transition.**

I. Introduction

PRECISION assembly and manipulation of objects with size ranging from microns to millimeters have drawn more and more attention in advanced manufacturing due to its significant advantages for applications in photoelectronic engineering, biotechnology, medical science, and microelectromechanism system [1]–[4]. In precision assembly, peg-in-hole assembly is a canonical operation [5]. Traditionally, a peg-in-hole assembly task can be divided into two substages, i.e., the alignment stage and the insertion stage [6]–[8]. The alignment of small components is realized based on microscopic vision, while in most cases, the insertion of components is achieved based on force servo control [9]. Visual servo control is dependent on accurate and precision pose estimation [10]. Many pose estimation methods have been reported in the literature, which could estimate the poses of components in six degrees of freedom (DOFs) in 3-D space both accurately and precisely [6]. In these pose estimation methods, mathematical models are established to express the pose projections from the image space to the Cartesian space. Based on these pose estimation methods, the alignment of components can be realized effectively.

However, the development of force servo control methods for insertion of components is a different situation in the domain of precision assembly. Currently, two kinds of force servo control methods are reported in the literature, i.e., the model based ones [11]–[16] and the model free ones [8]. The model-based force servo control methods try to find a mathematical model to explain the insertion process physically in order to understand the current status of the insertion process and adopt the corresponding control steps afterward. The established models usually do not work in high efficiency in reality due to the basic assumption in the force condition analysis that there is no machining error in the component manufacturing process. In addition, for different components, mathematical models for insertion are developed separately. For example, in [11], a method to direct admittance selection for force-guided assembly considering multiple-point contact is proposed. In [12], the passive admittance and associated maximum coefficient of friction is presented for planar force assembly of a variety of different polygonal parts. In [13], an active force control strategy for guiding tasks in microassembly together with the stability of grasp during contact is investigated. In [14], a robust impedance control approach for high-speed position and force regulation is presented for microgrippers dedicated to microassembly tasks. In [15], a hybrid control approach for vertical and horizontal precision assemblies among thin irregular objects performed by multiple manipulators is presented. These model-based insertion control methods mostly focused on and showed generality in realizing the assembly of components with various shapes or various fit types. However, these methods did not pay much attention in the efficiency. Besides, developing these models is time consuming and normally needs the developers to be familiar with the physical dynamics. For model free force servo control methods, the control strategy is based on some simple

Manuscript received September 11, 2016; revised December 29, 2017 and March 29, 2017; accepted May 9, 2017. Date of publication June 2, 2017; date of current version October 24, 2017. *(Corresponding author: Song Liu.)*

S. Liu and Y.-F. Li are with the City University of Hong Kong, Kowloon, Hong Kong (e-mail: sdliusong@outlook.com; meyfli@cityu.edu.hk).

D.-P. Xing, D. Xu, and H. Su are with the Research Center of Precision Sensing and Control, Institute of Automation, Chinese Academy of Sciences, Beijing 100190, China (e-mail: dengpeng.xing@ia.ac.cn; de.xu@ia.ac.cn; hu.su@ia.ac.cn).

Color versions of one or more of the figures in this paper are available online at http://ieeexplore.ieee.org.

Digital Object Identifier 10.1109/TIE.2017.2711551

constraint criteria. These criteria are set up for safety reasons to prevent the components from breakage. For example, in [8] and [15], for the assembly of thin annular components, the movement of component along the insertion direction will proceed only when the force conditions along the insertion-orthogonal directions are within the permitted range. These insertion control strategies control the insertion process conservatively due to the lack of assembly dynamics. Therefore, these methods are low in efficiency. Due to the discussion above, it is necessary to develop a universal force-guiding strategy for the peg-in-hole assembly tasks from a new perspective.

Both force-guided precision assembly and traditional assembly face the problem of uncertainty when trying to model the dynamics between the force state and the manipulator's position. However, precision assembly is different from the traditional assembly in several aspects [7]. First, in the domain of precision assembly, components are normally prealigned in Cartesian space in high precision to promise the final assembly precision. Thus, the ordinary jammed situation in traditionally assembly is rare in precision assembly. This property enable us to focus on the efficiency in developing insertion control strategy rather than dealing with the unusual insertion situations. Second, during the insertion process of components in precision assembly, the deformation of components is normally in several microns, and, thus, is within the elastic range of the components [9]. This is an important property compared with traditional assembly, which can be utilized to develop an efficient insertion control method. Finally, to guarantee the final assembly precision, the orientation of components is not permitted to adjust during the insertion process in the precision assembly. This difference confines us to realize insertion only with translation DOFs in precision assembly.

The uncertainty becomes more prominent in precision assembly due to the reason that the force states during the precision assembly process are normally in small range. The uncertainty arises from the machining errors of components, the observation noise of the force sensor, and the anisotropy of the components' material, etc. In traditional assembly, the uncertainty is usually described as Gaussian distribution or Gaussian mixture distribution. For example, in [17], Tang *et al*. train a Gaussian mixture to build a state-varying admittance block, which generates a similar velocity output given the same wrench input. In this case, the relationship between the input and the output is directly modeled by the Gaussian mixture, and the uncertainty relies on the unrecorded input–output pairs in the training dataset. In [18], an expectation maximization-based Gaussian mixture model (EM-GMM) is used to address the problem of contact-state recognition for force-guided robotic tasks. The EM-GMM works as a classifier to recognize different contact formations. In [19], the Gaussian method is used to identify the accurate hole position in force-guided robotic peg-in-hole assembly tasks. In these industrial applications, the Gaussian distribution can normally explain the random process well, and it also shows up excellent calculation property in inducing complicated control strategies. Based on these inspirations and deep analysis on historical insertion experiment data, we try to introduce this modeling approach into precision assembly of cylindrical components to describe the uncertainty during force state transition process caused by the control action. An efficient control method is also elaborately developed fully utilizing the properties of the Gaussian distribution.

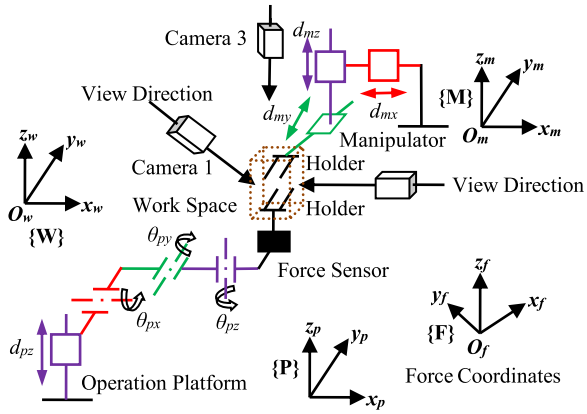

Fig. 1. Basic configuration of the assembly system.

The motivation of this paper is to develop an efficient insertion control strategy dedicated for cylindrical components with interference fit. Specifically, the insertion of components is modeled as a stochastic state transition process with the uncertainty described by the Gaussian distribution. Then, the state transition function is well defined based on the analysis of the historical assembly data and the universal mechanical properties of the components. An assessment function is also elaborately designed to assess the performance of the state transition function. Finally, the action to be taken for the current state is decided by iterative calculations in N steps estimation manner. An automatic assembly system is developed to verify the effectiveness of the proposed insertion control method.

The remainder of this paper is organized as follows. Section II first gives an introduction of the system setup on which the proposed insertion control strategy is verified. In Section III, modeling process including the state transition function and the assessment function are provided. Then, details of the insertion control strategy are discussed in Section IV. Section V presents the experiments and results of the proposed strategy. Finally, this paper is concluded in Section VI.

II. System Configuration

The insertion control strategy proposed in this paper is discussed and unfolded under the basic assembly system configuration, as shown in Fig. 1. In Fig. 1, $\{\mathbf{W}\}$ is the world coordinate system, $\{\mathbf{F}\}$ is the force coordinate system, $\{\mathbf{P}\}$ is the operation platform coordinate system, and $\{\mathbf{M}\}$ is the manipulator coordinate system. The assembly system includes three cameras to measure the relative pose of components in 5 **DOF**s (attitude around z_w-axis excluded), an operation platform consisting of three rotation **DOF**s and one elevating **DOF** to align one component to the other in attitude, a manipulator consisting of three translation **DOF**s to align one component to the other

in position, and a force sensor to measure the contact forces between the components in the insertion process in three orthogonal directions. The force sensor can either be mounted under the holder on the operation platform or upon the holder on the manipulator.

The alignment of the components is achieved according to the alignment scheme developed in [8]. Since this paper focuses on developing an efficient insertion control strategy, the components to be assembled are always supposed to have been aligned in advance. In principle, the insertion of the components can be implemented via either moving up one component along the z_p-axis or moving down the other along the z_m-axis. In consideration of the force modification problem of f_x and f_y, the insertion process is achieved by the manipulator. Under the proposed system configuration, the insertion process can be described as increasing the contact force along z_f-axis to a threshold value asymptotically, while keeping the forces along $x_f\, y_f$ plane in a limited range to avoid unexpected deformation or even breakage of the components.

III. Mathematical Description of an Insertion Process

The insertion process is described as a five tuple

$$\{\boldsymbol{S}, \boldsymbol{A}, \boldsymbol{P}(\boldsymbol{s}_k, \boldsymbol{a}_k, \boldsymbol{s}_{k+1}), \boldsymbol{R}(\boldsymbol{s}_k, \boldsymbol{a}_k, \boldsymbol{s}_{k+1}), \gamma\} \tag{1}$$

where $\boldsymbol{s}$ is the state of the observed process, $\boldsymbol{a}$ is the action taken by the control system, k is the control step index, $\boldsymbol{S}$ is the finite set of states, $\boldsymbol{A}$ is the finite set of actions, $\boldsymbol{P}(\boldsymbol{s}_k, \boldsymbol{a}_k, \boldsymbol{s}_{k+1}) = \boldsymbol{P}(\boldsymbol{s}_{k+1}|\boldsymbol{s}_k, \boldsymbol{a}_k)$ is the state transition function describing the probability that action $\boldsymbol{a}_k$ in state $\boldsymbol{s_k}$ at the $\boldsymbol{k}$th control step will lead to state $\boldsymbol{s}_{k+1}$, $\boldsymbol{R}(\boldsymbol{s}_k, \boldsymbol{a}_k, \boldsymbol{s}_{k+1})$ is the assessment function evaluating the performance of the state transition to state $\boldsymbol{s_{k+1}}$ from state $\boldsymbol{s_k}$, and γ is the discount factor, which determines the strategy controlling the insertion process progressively or conservatively $0 < \gamma < 1$.

For the insertion control problem in precision assembly tasks, the contact condition between the components is monitored by the force sensor and the state is composed of the forces along $\boldsymbol{x_f}$-, $\boldsymbol{y_f}$- and $\boldsymbol{z_f}$-axis given as

$$\boldsymbol{s}_k = [f_x, f_y, f_z]_k^{\mathrm{T}}. \tag{2}$$

The action the control system takes for current state $\boldsymbol{s}_k$ to promote the insertion process is given by

$$\boldsymbol{a}_k = [d_{mx}, d_{my}, d_{mz}]_k^{\mathrm{T}}. \tag{3}$$

The insertion process is to make movement decision $\boldsymbol{a}_k$ according to the current state $\boldsymbol{s}_k$ in order to asymptotically transit the state from start state $\boldsymbol{s}_0$ to the end $\boldsymbol{s}_K$ based on the state transition function and the assessment function. The $\boldsymbol{s}_0$ and $\boldsymbol{s}_K$ are given as follows:

$$\boldsymbol{s}_0 = [0, 0, 0]^{\mathrm{T}},\ \boldsymbol{s}_K = [0, 0, F_z]^{\mathrm{T}} \tag{4}$$

where F_z is the threshold value.

As the discussion above, the state transition function and the assessment function play significant roles in the decision-making process. The following part of this section will focus on the development of the state transition function and the design of the assessment function.

A. State Transition Function

For solid materials, when the deformation is within the elastic limit, the relationship between the force exerted on the material and the deformation can be expressed by

$$\Delta L = \frac{L}{SE} F \tag{5}$$

where F is the force exerted, L is the length of the material, S is the cross-sectional area, and E is the Young modulus of the material. For most millimeter level size components in precision assembly, when the deformation is within several microns, the relationship between the contact force among the components and the deformation of the components satisfies (5).

It should be emphasized that (5) expresses a linear relationship. If the force exerted on the material and the deformation of the material are decoupled into three orthogonal directions in $\{\mathbf{F}\}$ and $\{\mathbf{M}\}$, respectively, (5) can be represented in matrix form as given by

$$\begin{bmatrix} \Delta L_{mx} \\ \Delta L_{my} \\ \Delta L_{mz} \end{bmatrix} = \frac{L}{SE} \boldsymbol{R} \begin{bmatrix} f_x \\ f_y \\ f_z \end{bmatrix} = \boldsymbol{J} \begin{bmatrix} f_x \\ f_y \\ f_z \end{bmatrix} \tag{6}$$

where $\boldsymbol{R}$ is the conversion matrix from $\{\mathbf{F}\}$ to $\{\mathbf{M}\}$. For cylindrical components, the mechanical properties show isotropy due to the isotropy in physical structure. Therefore, the parameters of L, S, and E in (6) are constants in different radial directions. If the spindle of the component is parallel with the $\boldsymbol{z_m}$-axis, the transformation matrix $\boldsymbol{J}$ in (6) will also be constant.

It is difficult and impractical to measure the micron level deformations of a solid component in millimeter level size. However, for cylindrical components with interference fit under the insertion process, the decoupled elements of the variation of the deformation of the components in $\{\mathbf{M}\}$ can be approximately replaced by the movement increments of the manipulator. Therefore, (6) is rewritten as

$$\begin{bmatrix} d_{mx} \\ d_{my} \\ d_{mz} \end{bmatrix} = \boldsymbol{J} \begin{bmatrix} \Delta f_x \\ \Delta f_y \\ \Delta f_z \end{bmatrix}. \tag{7}$$

There are many factors influencing the reliability of (7), such as using the movement increments of the manipulator to replace the deformation of the components in $\{\mathbf{M}\}$, the measurement error and of the force sensor, and the unstrictly parallel relationship between the spindle of the components and the $\boldsymbol{z_m}$-axis. All the factors can be viewed as noises and modeled as an uncertain item into (7). Therefore, for a state $\boldsymbol{s_k}$ and an action $\boldsymbol{a}_k$, the $\boldsymbol{s_{k+1}}$ can be estimated by

$$\boldsymbol{s}_{k+1} = \boldsymbol{s}_k + \boldsymbol{J}^{-1} \boldsymbol{a}_k + \boldsymbol{\tau} \tag{8}$$

where τ is the uncertain item. It is reasonable to assume that τ obeys normal distribution; in fact, it is verified in Section V.

The state transition function for the insertion process of cylindrical components is given by

$$\begin{aligned}&\boldsymbol{P}(\boldsymbol{s}_{k+1}|\boldsymbol{s}_k,\boldsymbol{a}_k)\\&=\frac{1}{(2\pi)^{\frac{3}{2}}}\frac{1}{|\sum|^{\frac{1}{2}}}\exp\Big(-\frac{1}{2}(\boldsymbol{s}_{k+1}-\boldsymbol{s}_k-\boldsymbol{J}^{-1}\boldsymbol{a}_k\Big)^T\\&\quad\sum{}^{-1}(\boldsymbol{s}_{k+1}-\boldsymbol{s}_k-\boldsymbol{J}^{-1}\boldsymbol{a}_k))\\&=\mathcal{N}\Big(\boldsymbol{s}_k+\boldsymbol{J}^{-1}\boldsymbol{a}_k,\sum\Big)\end{aligned}\tag{9}$$

where Σ is the 3×3 variance matrix. To get the $\boldsymbol{J}$ and Σ in (9), the insertion process need first be conducted manually to get a set of training data in which the movement increments and the corresponding force variations are recorded. The $\boldsymbol{J}$ is computed with least square method based on (7). Afterward, Σ can be calculated by analyzing the estimation performance of the $\boldsymbol{J}$.

B. Assessment Function

The assessment function evaluates the performance of the state transition function in describing the state transition process in last control step so that the strategy makes decision accordingly. For the state transition process from $\boldsymbol{s}_0$ and $\boldsymbol{s}_K$, the control system is expected to increase the force along $\boldsymbol{z_f}$-axis to F_z asymptotically, while the forces in $\boldsymbol{x_f}\,\boldsymbol{y_f}$ plane are expected to be as small as possible. In other words, safety and efficiency are the two most important assessment criteria, which, therefore, are the core principles to design the assessment function. However, safety is contradictory to efficiency to some extent. For the sake of safety, if the offset vector formed by the f_x and f_y of the state $\boldsymbol{s_{k+1}}$ is far away from the balance point $(0, 0)^{\mathrm{T}}$, the state transition function should be evaluated negatively in describing the state transition process in last control step; while for the sake of efficiency, if the insertion depth $|d_{mz}|$ is relatively larger under the same offset vector formed by the f_x and f_y of the state $\boldsymbol{s_{k+1}}$, the state transition function should be evaluated positively in describing the state transition process in last control step. If both of the above circumstances happen, the assessment function needs to evaluate how serious is the mistake and how great is the contribution caused by the state transition in last control step. The positive correlation relationship is given in

$$\boldsymbol{R}(\boldsymbol{s}_k,\boldsymbol{a}_k,\boldsymbol{s}_{k+1})\propto\frac{\sqrt{f_x^2+f_y^2}}{|d_{mz}|}.\tag{10}$$

Concrete value assignment to the reward function depends on the tradeoff between the safety and efficiency, which is highly effected by the performance of the state transition function. If the Gaussian distribution in (9) is tight, we can pay more attention to the efficiency. Otherwise, the safety should be considered more seriously.

The assessment function is mainly used to update the γ factor in (1) and the force increment Δf_{z1} which is discussed in detail in the following Section IV-C, and in Section V, the assessment function is assigned specific values in a table.

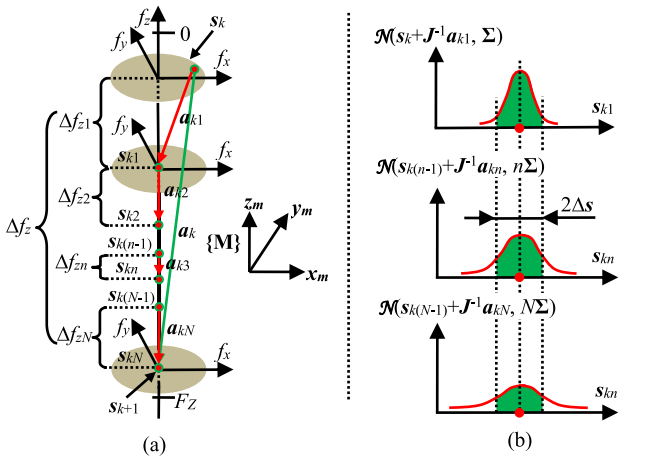

Fig. 2. *N* steps action estimation approach.

IV. Insertion Control

A. N Steps Action Estimation Approach

The core of the proposed insertion control method is to make decision for the action $\boldsymbol{a}_k$ which is to be taken for current state $\boldsymbol{s_k}$. To estimate the action which transits the state from $\boldsymbol{s}_k$ to $\boldsymbol{s}_{k+1}$, the state $\boldsymbol{s}_{k+1}$ need first be figured out so that the action can be calculated according to the state difference and the state transition function. The key difference between $\boldsymbol{s}_k$ and $\boldsymbol{s}_{k+1}$ relies on the force increment Δf_z. From the perspective of efficiency, the Δf_z should be determined accordingly rather than being set manually or preliminarily. Detailed setting strategy for the Δf_z is discussed in Section IV-C.

It should be pointed out that one of the preconditions for the state transition function to work is the movement increment of each action should not be too large for the reason that large movement increments may cause nonlinear force increments. Therefore, a method to compensate the nonlinearity or uncertainty between the force increments and large movement increments is needed. In this section, an *N* steps estimation approach is proposed, in which a large force increment Δf_z is divided into *N* small force increments and the uncertainty caused by large movement increment is compensated by increasing loose Gaussian distribution.

1) First Step Action Estimation: As shown in Fig. 2(a), a large force increment Δf_z is divided into *N* small force increments, such as Δf_{z1}, Δf_{z2} … Δf_{zn} … Δf_{zN}, and the corresponding state is denoted as $\boldsymbol{s}_{k1}$, $\boldsymbol{s}_{k2}$ … $\boldsymbol{s}_{kn}$ … $\boldsymbol{s}_{kN}$. The first step estimation is dedicated for force increment Δf_{z1}.

The state difference $\Delta\boldsymbol{s}$ is first calculated by subtracting $\boldsymbol{s}_k$ from $\boldsymbol{s}_{k1}$. Then, the action $\boldsymbol{a}_{k1}$ transits $\boldsymbol{s}_k$ to $\boldsymbol{s}_{k1}$ is computed by (7). According to the state transition function, the conditional distribution of the state $\boldsymbol{s}_{k1}$ is given directly by

$$\boldsymbol{P}(\boldsymbol{s}_{k1}|\boldsymbol{s}_k,\boldsymbol{a}_{k1})=\mathcal{N}\Big(\boldsymbol{s}_{k1}|\boldsymbol{s}_k+\boldsymbol{J}^{-1}\boldsymbol{a}_{k1},\sum\Big).\tag{11}$$

2) Second Step Action Estimation: The second step estimation is to calculate the action $\boldsymbol{a}_{k2}$ which transits the state from $\boldsymbol{s}_{k1}$ to $\boldsymbol{s}_{k2}$. The difference between $\boldsymbol{s}_{k1}$ and $\boldsymbol{s}_{k2}$ is the force

increment of Δf_{z2}. If $\boldsymbol{s}_{k1}$ is a specific state like $\boldsymbol{s}_k$, the action $\boldsymbol{a}_{k2}$ can be directly computed by (7). However, $\boldsymbol{s}_{k1}$ follows the conditional Gaussian distribution as given in (11), which leads to a result that $\boldsymbol{a}_{k2}$ will also follow a probabilistic distribution as given by

$$\boldsymbol{P}(\boldsymbol{a}_{k2} = \boldsymbol{J}(\boldsymbol{s}_{k2} - \boldsymbol{s}_{k1})) = \boldsymbol{P}(\boldsymbol{s}_{k1}|\boldsymbol{s}_k, \boldsymbol{a}_{k1}). \tag{12}$$

The final decision for the action $\boldsymbol{a}_{k2}$ is computed as the expectation of all possible values of $\boldsymbol{a}_{k2}$ as given by

$$\boldsymbol{a}_{k2} = \int \boldsymbol{P}(\boldsymbol{s}_{k1}|\boldsymbol{s}_k, \boldsymbol{a}_{k1})\boldsymbol{J}(\boldsymbol{s}_{k2} - \boldsymbol{s}_{k1})d\boldsymbol{s}_{k1}. \tag{13}$$

Utilizing the symmetric property of the Gaussian distribution, the action $\boldsymbol{a}_{k2}$ is computed as

$$\boldsymbol{a}_{k2} = \boldsymbol{J}(\boldsymbol{s}_{k2} - \boldsymbol{s}_{k1})\Big|_{\boldsymbol{s}_{k2} = E(\boldsymbol{s}_{k1}) + [0,0,\Delta f_{z2}]^{\mathrm{T}}} \tag{14}$$

where $E(\boldsymbol{s}_{k1})$ is the expectation of the $\boldsymbol{s}_{k1}$.

What is paid more attention to is the distribution of $\boldsymbol{s}_{k2}$ once the action $\boldsymbol{a}_{k1}$ and $\boldsymbol{a}_{k2}$ are taken successively. From a specific state $\boldsymbol{s}_{k1}$, the probabilistic distribution of $\boldsymbol{s}_{k2}$ is the same Gaussian distribution as $\boldsymbol{s}_{k1}$ in (11). Therefore, for a specific state of $\boldsymbol{s}_{k2}$, its corresponding probability is the integration of all the possibilities that the action $\boldsymbol{a}_{k2}$ transits the state from all possible $\boldsymbol{s}_{k1}$ to $\boldsymbol{s}_{k2}$, as given by

$$\begin{aligned}&\boldsymbol{P}(\boldsymbol{s}_{k2}|\boldsymbol{s}_{k1}, \boldsymbol{a}_{k2})\\ &= \int \mathcal{N}\Big(\boldsymbol{s}_{k2}|\boldsymbol{s}_{k1} + \boldsymbol{J}^{-1}\boldsymbol{a}_{k2}, \sum\Big)\\ &\quad \times \mathcal{N}\Big(\boldsymbol{s}_{k1}|\boldsymbol{s}_k + \boldsymbol{J}^{-1}\boldsymbol{a}_{k1}, \sum\Big)\, d\boldsymbol{s}_{k1}.\end{aligned} \tag{15}$$

The central position or mean value point of the distribution of the state $\boldsymbol{s}_{k2}$ is linearly determined by $\boldsymbol{s}_{k1}$. If the $\boldsymbol{s}_{k2}$ is translated by $-\boldsymbol{s}_{k1}$, (15) can be transformed into

$$\begin{aligned}&\boldsymbol{P}(\boldsymbol{s}_{k2}|\boldsymbol{s}_{k1}, \boldsymbol{a}_{k2})\\ &= \int \mathcal{N}\Big(\boldsymbol{s}_{k2} - \boldsymbol{s}_{k1}|\boldsymbol{J}^{-1}\boldsymbol{a}_{k2}, \sum\Big)\\ &\quad \times \mathcal{N}\Big(\boldsymbol{s}_{k1}|\boldsymbol{s}_k + \boldsymbol{J}^{-1}\boldsymbol{a}_{k1}, \sum\Big)\, d\boldsymbol{s}_{k1}.\end{aligned} \tag{16}$$

Based on the definition of convolution, the probabilistic distribution of the state $\boldsymbol{s}_{k2}$ is the convolution of two Gaussian distributions as given by

$$\begin{aligned}\boldsymbol{P}(\boldsymbol{s}_{k2}|\boldsymbol{s}_{k1}, \boldsymbol{a}_{k2}) &= \mathcal{N}\Big(\boldsymbol{s}_{k2}|\boldsymbol{J}^{-1}\boldsymbol{a}_{k2}, \sum\Big)\\ &\quad * \mathcal{N}\Big(\boldsymbol{s}_{k2}|\boldsymbol{s}_k + \boldsymbol{J}^{-1}\boldsymbol{a}_{k1}, \sum\Big).\end{aligned} \tag{17}$$

According to the convolution theorem, the Fourier transform of the convolution of two functions is the product of the Fourier transform of each function. Therefore, conducting Fourier transform on both sides of (17) yields

$$\begin{aligned}&\mathscr{F}(\boldsymbol{P}(\boldsymbol{s}_{k2}|\boldsymbol{s}_{k1}, \boldsymbol{a}_{k2}))\\ &= \mathscr{F}\left(\mathcal{N}\Big(\boldsymbol{s}_{k2}|\boldsymbol{J}^{-1}\boldsymbol{a}_{k2}, \sum\Big)\right)\\ &\quad \times \mathscr{F}\left(\mathcal{N}\Big(\boldsymbol{s}_{k2}|\boldsymbol{s}_k + \boldsymbol{J}^{-1}\boldsymbol{a}_{k1}, \sum\Big)\right).\end{aligned} \tag{18}$$

Based on the shift property, (18) equals

$$\begin{aligned}&\mathscr{F}(\boldsymbol{P}(\boldsymbol{s}_{k2}|\boldsymbol{s}_{k1}, \boldsymbol{a}_{k2}))\\ &= A\mathcal{N}\Big(j\boldsymbol{\omega}|\vec{\boldsymbol{0}}, \sum{}^{-1}\Big)\\ &\quad \times \mathcal{N}\Big(j\boldsymbol{\omega}|\vec{\boldsymbol{0}}, \sum{}^{-1}\Big)\, e^{-j\boldsymbol{\omega}(\boldsymbol{J}^{-1}\boldsymbol{a}_{k2})} e^{-j\boldsymbol{\omega}(\boldsymbol{s}_k + \boldsymbol{J}^{-1}\boldsymbol{a}_{k1})}\end{aligned} \tag{19}$$

where A represents the coefficient. Further derivation of (19) yields

$$\begin{aligned}&\mathscr{F}(\boldsymbol{P}(\boldsymbol{s}_{k2}|\boldsymbol{s}_{k1}, \boldsymbol{a}_{k2}))\\ &= A\mathcal{N}\Big(j\boldsymbol{\omega}|\vec{\boldsymbol{0}}, \frac{1}{2}\sum{}^{-1}\Big)\, e^{-j\boldsymbol{\omega}(\boldsymbol{s}_k + \boldsymbol{J}^{-1}\boldsymbol{a}_{k1} + \boldsymbol{J}^{-1}\boldsymbol{a}_{k2})}.\end{aligned} \tag{20}$$

Conducting inverse Fourier transform to (20) yields the probabilistic distribution of the state $\boldsymbol{s}_{k2}$ as given by

$$\boldsymbol{P}(\boldsymbol{s}_{k2}|\boldsymbol{s}_{k1}, \boldsymbol{a}_{k2}) = \mathcal{N}\Big(\boldsymbol{s}_{k2}|\boldsymbol{s}_k + \boldsymbol{J}^{-1}\boldsymbol{a}_{k1} + \boldsymbol{J}^{-1}\boldsymbol{a}_{k2}, 2\sum\Big). \tag{21}$$

3) nth Step Action Estimation: Without the loss of generality, the results of the second step action estimation given in (14) and (21) can be generalized into the *n*th step estimation. The *n*th step action is given in

$$\boldsymbol{a}_{kn} = \boldsymbol{J}(\boldsymbol{s}_{kn} - \boldsymbol{s}_{k(n-1)})\Big|_{\boldsymbol{s}_{kn} = E(\boldsymbol{s}_{k(n-1)}) + [0,0,\Delta f_{zn}]^{\mathrm{T}}}. \tag{22}$$

The probabilistic distribution of the state $\boldsymbol{s}_{kn}$ of the *n*th step estimation is given in

$$\boldsymbol{P}(\boldsymbol{s}_{kn}|\boldsymbol{s}_{k(n-1)}, \boldsymbol{a}_{kn}) = \mathcal{N}\left(\boldsymbol{s}_k + \boldsymbol{J}^{-1}\sum_{i=1}^{n}\boldsymbol{a}_{ki}, n\sum\right). \tag{23}$$

The generalization from (14) and (21) to the results of (22) and (23) can be verified by the mathematical induction method.

If the estimation depth is *N*, the action $\boldsymbol{a}_k$ dedicated for current state $\boldsymbol{s}_k$ is decided as the vector sum of the $\boldsymbol{a}_{kn}$ as given in

$$\boldsymbol{a}_k = \sum_{n=1}^{N}\boldsymbol{a}_{kn}. \tag{24}$$

The distribution of the state $\boldsymbol{s}_{k+1}$ once the action $\boldsymbol{a}_k$ is taken can be got by simply substituting the *n* with *N* in (23).

B. Determination of Estimation Depth and Force Increments

From (23), it can be seen that as the iterative estimation gets deeper and deeper, the variance and covariance elements in the variance matrix become linearly larger and larger. As a result, the Gaussian distribution of the state is getting increasing loose as shown in Fig. 2(b), which means that it is more and more difficult to confine the expected state within a limited range.

As shown in Fig. 2(b), the area of the green region centered at the mean point of the Gaussian distribution and confined by $\Delta \boldsymbol{s}$ is the probability that the coming state $\boldsymbol{s}_{kn}$ is located in the acceptable error range. The area of the green region gets increasingly small as N increases. This probability is expected to be no less than a threshold as given by

$$\int_{\boldsymbol{s}=\boldsymbol{s}_{kn}-\Delta \boldsymbol{s}}^{\boldsymbol{s}=\boldsymbol{s}_{kn}+\Delta \boldsymbol{s}} \boldsymbol{P}(\boldsymbol{s}_{kn}|\boldsymbol{s}_{k(n-1)}, \boldsymbol{a}_{k(n-1)})d\boldsymbol{s} \geq T_s \tag{25}$$

where T_s is the threshold. The above inequation is dominated by three parameters such as the $\Delta \boldsymbol{s}$, T_s, and n. This is an important property that can be utilized in the insertion action decision process. Once $\Delta \boldsymbol{s}$ and T_s are set, the estimation depth N is the largest n which satisfies the inequation.

As discussed in Section IV-A, a large force increment Δf_z is divided into small force increments Δf_{zn} to compensate the nonlinearity caused by large movement increments. However, Δf_z is not appointed in advance and then divided according to the estimation depth N. Actually, the Δf_{zn} is calculated individually according to the method introduced in this section.

For the kth control step, the force increment $(\Delta f_{z1})_k$ is determined according to the force increment $(\Delta f_{z1})_{k-1}$ and the assessment value $\boldsymbol{R}(\boldsymbol{s}_{k-1}, \boldsymbol{a}_{k-1}, \boldsymbol{s}_k)$. The determination of $(\Delta f_{z1})_k$ is concerned with the working mechanism of the proposed control strategy, which is discussed in Section IV-C.

The following force increments $(\Delta f_{zn})_k$ is set based on the $(\Delta f_{z1})_k$ and the γ factor, which is calculated by

$$(\Delta f_{zn})_k = \gamma(\Delta f_{z(n-1)})_k,\ 1 < n \leq N. \tag{26}$$

The γ factor is used to optimize or maximize the assessment function to seek the best action for current state. It can reflect the strategy confidence on the performance of the state transition function. It is updated after every control step according to the immediate state transition assessment value which is discussed also in Section IV-C.

C. Insertion Control

Based on the discussion above, the insertion control procedure is proposed in detail in this section. The setting of the assessment function always encourages the controller to achieve the best efficiency no matter how much the safety principle is stressed, which means the action estimation approach in every control step always tries to find the best action with the largest possible insertion depth. According to (22) and (24), the largest possible insertion depth is mainly dominated by parameters such as the estimation depth N and the force increments Δf_{zn}. The efficiency of the action decision approach is highly affected by the four independent parameters of Δf_{z1}, γ, $\Delta \boldsymbol{s}$, and T_s. How to set the above parameters is mainly concerned with the performance of a state transition function, which is evaluated by the assessment function. If the state transition in last control step is evaluated with a high positive value, the state transition function can be believed to perform well. Therefore, the strategy can estimate the action $\boldsymbol{a}_k$ more confidently. In such circumstance, the parameters of Δf_{z1}, γ, $\Delta \boldsymbol{s}$, and T_s can be set to be larger. In the contrary, if the state transition in last control step is assessed with a high negative value, the state transition function is believed to perform poorly. Therefore, the strategy can estimate the action $\boldsymbol{a}_k$ more conservatively. In such case, the parameters of Δf_{z1}, γ, $\Delta \boldsymbol{s}$, and T_s can be set smaller.

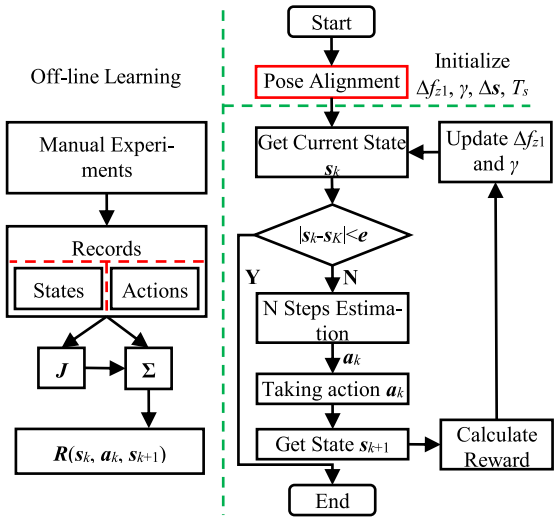

Fig. 3. Flowchart of the insertion control strategy.

The insertion control strategy proposed in this paper chooses the parameters of Δf_{z1} and γ to be set accordingly as given in (27), while $\Delta \boldsymbol{s}$ and T_s are fixedly set in advance

$$\begin{aligned}(\Delta f_{z1})_k &= (1 + \boldsymbol{R}(\boldsymbol{s}_{k-1}, \boldsymbol{a}_{k-1}, \boldsymbol{s}_k))(\Delta f_{z1})_{k-1}, \\ &\quad \times\ F_1 < (\Delta f_{z1})_k < F_2 \\ (\gamma)_k &= (1 + \boldsymbol{R}(\boldsymbol{s}_{k-1}, \boldsymbol{a}_{k-1}, \boldsymbol{s}_k))(\gamma)_{k-1},\ \gamma_1 < \gamma < \gamma_2\end{aligned} \tag{27}$$

where F_1, F_2, γ_1, and γ_2 are thresholds. The use of the assessment function in (27) imposes a limitation on the range of (10) to be $[-1, 1]$.

As a conclusion of the proposed method, Fig. 3 outlines the whole idea for insertion control. First, manual experiments are conducted to record the state–action pairs for the learning or calibration of the matrices $\boldsymbol{J}$ and Σ in the state transition function. Afterward, values are assigned to the assessment function based on the analysis of the covariance matrix Σ.

For every insertion task, the components are first aligned in 5 DOF by the vision-based method [8] in order to get ready for insertion. Then, the parameters of Δf_{z1} and γ are initialized for the first control step and the $\Delta \boldsymbol{s}$ and T_s for the whole task. For the kth insertion control step, the current state $\boldsymbol{s}_k$ is first captured from the force sensor. Then, the state difference between the state $\boldsymbol{s}_k$ and the target state $\boldsymbol{s}_K$ is calculated. If the difference is less than a threshold $\boldsymbol{e}$, the insertion task is finished. Otherwise, the action $\boldsymbol{a_k}$ for current state $\boldsymbol{s}_k$ is estimated by the N steps estimation method. After taking the action $\boldsymbol{a}_k$, the state $\boldsymbol{s}_{k+1}$ is captured from the force sensor to calculate the assessment value for the state transition. Finally, the parameters of Δf_{z1} and γ are updated for the next control step.

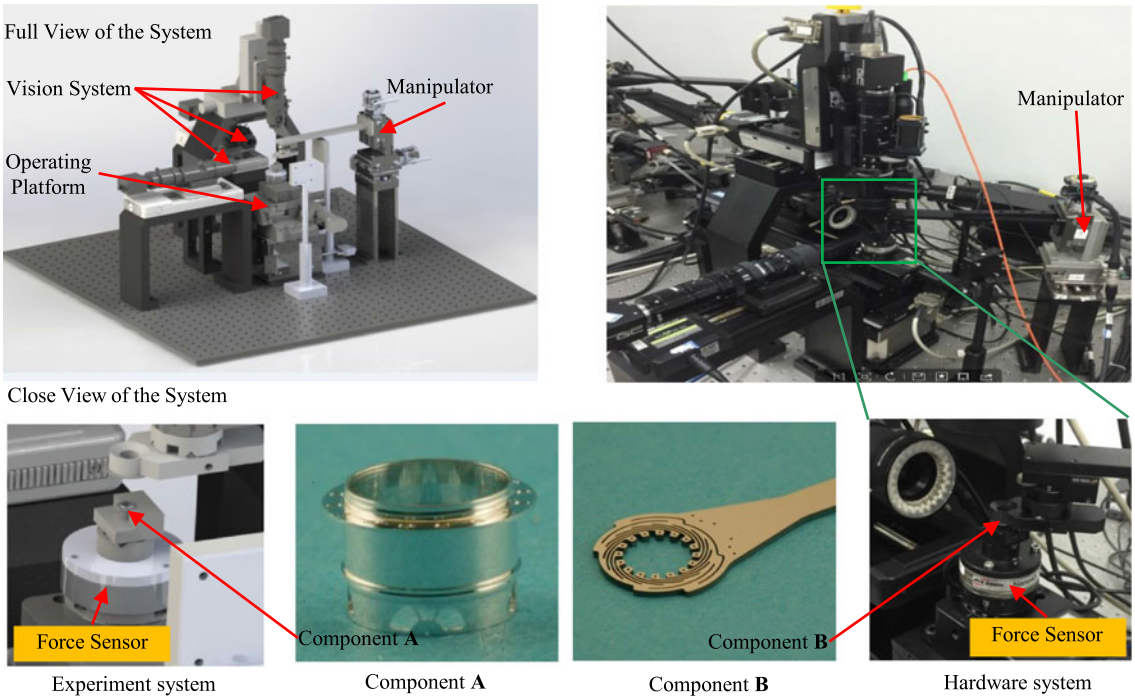

Fig. 4. Experiment system and components.

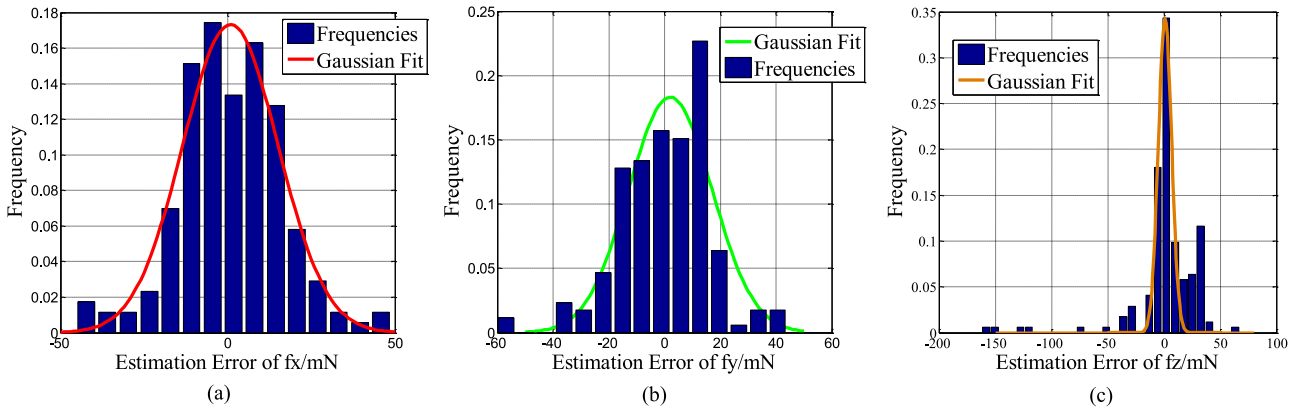

Fig. 5. Gaussian distribution verification of the estimation errors. (a) Goodness of fit $r^2 = 0.94$. (b) Goodness of fit $r^2 = 0.83$. (c) Goodness of fit $r^2 = 0.84$.

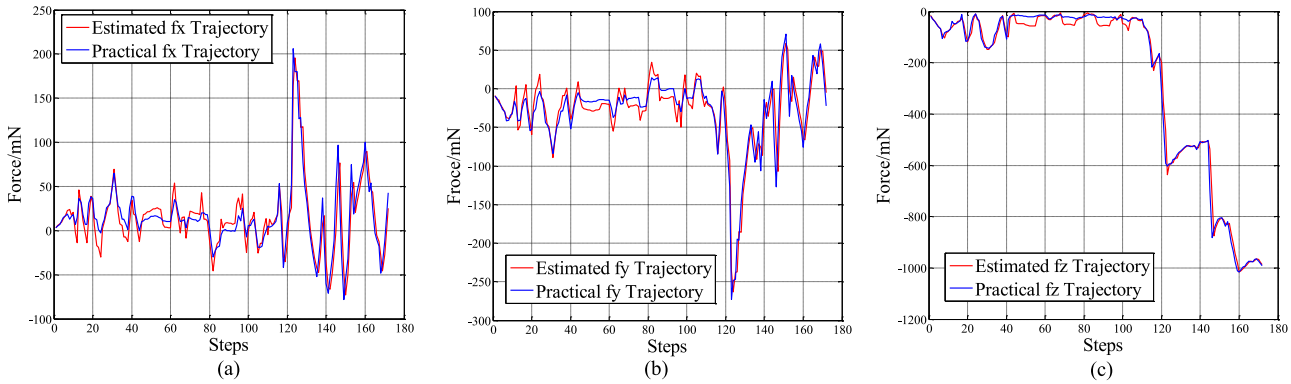

Fig. 6. Verification of model accuracy. (a) Trajectory of f_x. (b) Trajectory of f_y. (c) Trajectory of f_z.

TABLE I
VALUE ASSIGNMENT FOR REWARD FUNCTION

$\|\|f_x, f_y\|\|_2$ / $\|d_{mz}\|/\mu$m	[0, 15]	(15, 30]	(30, 45]	(45, 60]	>60
[0, 5]	0.05	0.025	−0.20	−0.70	−0.90
(5, 10]	0.10	0.05	−0.10	−0.70	−0.90
(10, 15]	0.15	0.10	0	−0.70	−0.90
(15, 20]	0.20	0.15	0.05	−0.70	−0.90
(20, 25]	0.25	0.20	0.10	−0.70	−0.90
>25	0.30	0.25	0.15	−0.70	−0.90

TABLE II
EXPERIMENT RESULTS IN ONE INSERTION TASK

Step	Δf_{z1}	γ	R	Step	Δf_{z1}	γ	R	Step	Δf_{z1}	γ	R
1	−20	0.2	0.15	7	−50	0.4	0.3	13	−50	0.4	0.25
2	−23	0.23	0.1	8	−50	0.4	0.3	14	−50	0.4	0.25
3	−25	0.25	0.1	9	−50	0.4	0.3	15	−50	0.4	0.15
4	−28	0.28	0.2	10	−50	0.4	0.3	16	−50	0.4	0.25
5	−33	0.33	0.2	11	−50	0.4	0.3	17	−50	0.4	−0.9
6	−40	0.4	0.3	12	−50	0.4	0.25	18	END	END	END

V. EXPERIMENTS AND RESULTS

A. Experimental Setup

An experiment system was set up according to the system configuration given in Section II, as shown in Fig. 4. In this experiment system, there were three microscopic cameras including two GC2450 cameras and one PointGrey camera. All three cameras were equipped with Navitar zoom lens with magnification $0.47 - 4.5\times$, which captured images 15 frames/s with image size of 2448 $\times$ 2050 pixels. The adjusting platform was composed of a Micos WT-100 for rotation around $\boldsymbol{X_w}$- and $\boldsymbol{Y_w}$-axis and a Sigma SGSP-40YAW for rotation around $\boldsymbol{Z_w}$-axis. The force sensor was Nano-43, which had measuring range of $\pm$18 N and resolution of 1/128 N along the X_w-, Y_w-, and Z_w--axis, respectively. Its signal was in a near-zero noise disturbance. A low-pass filter combining a Butterworth filter and a mean value filter was designed to filter the force signals. The force signals were first filtered by the Butterworth filter, then filtered by the mean filter. The random noise after filtering was in the range −5–5 mN. The window of the mean value filter was 50. Detailed parameters of the force filter were given in [8]. The manipulator was a Suguar KWG06030-G, whose translation resolution was 1 μm along $\boldsymbol{X_w}-$, $\boldsymbol{Y_w}$- and $\boldsymbol{Z_w}$-axis respectively. The CPU of the host computer was Intel Core$^{\text{TM}}$2 DUO.

The two components to be assembled were shown in Fig. 4. Component **A** was a cylindrical structure object with external diameter of 6 mm and height of 6 mm, while component **B** was a thin annular structure silicon object with external diameter of approximately 11 mm and thickness of 0.5 mm. The external diameter of upper end of the component **A** was 20 μm larger than the internal diameter of the component **B**. So the assembly of the components **A** and **B** was interference fit. There was an incline guidance surface at the top edge of the component **A**. Its height was 60 μm; it inclined about 30° from the vertical direction. The internal diameter of the component **B** could be stretched about 40 μm theoretically. The assembly task was to insert the component **A** into the component **B** in the condition that the surfaces of the two components were parallel to each other. The proposed insertion control method was verified on the established assembly system with the components **A** and **B**.

B. Learning of State Transition Function

To learn the state transition function, the insertion task was carried out four times manually with four different components

Fig. 7. Assembled component.

to record the state–action pairs as training and testing datasets. Then, based on the least square method and (7), the matrix $\boldsymbol{J}$ and the covariance matrix Σ were calculated with results given in

$$\boldsymbol{J} = \begin{bmatrix} -0.2411 & -0.2592 & 0.0263 \\ 0.0427 & -0.0700 & 0.0342 \\ -0.0051 & 0.1389 & -0.3610 \end{bmatrix} \mu\text{m/mN}$$

$$\sum = \begin{bmatrix} 241 & -206 & -177 \\ -206 & 257 & 254 \\ -177 & 254 & 808 \end{bmatrix} \text{mN}^2. \quad (28)$$

With $\boldsymbol{J}$ and Σ calibrated, the assumption of the Gaussian distribution of the uncertain item in the state transition function in (9) and the accuracy of the linear model in (7) were verified on testing dataset. For the reason of intuition, the Gaussian assumption was verified in the f_x-, f_y-, and f_z- dimensions individually. As shown by the bars in Fig. 5, the estimation errors were organized into groups with interval of 7 mN which is the resolution of the force sensor. Then, the frequencies were fit into Gaussian curves. Fig. 5(a)–(c) showed the fitting results of the force f_x, f_y, and f_z, respectively. The goodness of fit was measured by the r-square. The Gaussian fitting explained more than 80% of the frequency variation. It should be pointed out that the state transition function is expected to reflect the average state transition process of different components of the same kind so that the strategy shows repeatability in dealing with the assembly of components. In this sense, the state transition function does not need to be recalibrated frequently. The experiment result shown in Fig. 5 was produced from testing dataset which was generated from the assembly of other different components. Theoretically, it is not expected that the frequencies fit the Gaussian distribution completely. If the frequencies totally agree with the Gaussian distribution, it will cause overfitting problem, which means the state transition function captures all the observation noises and components manufacturing errors.

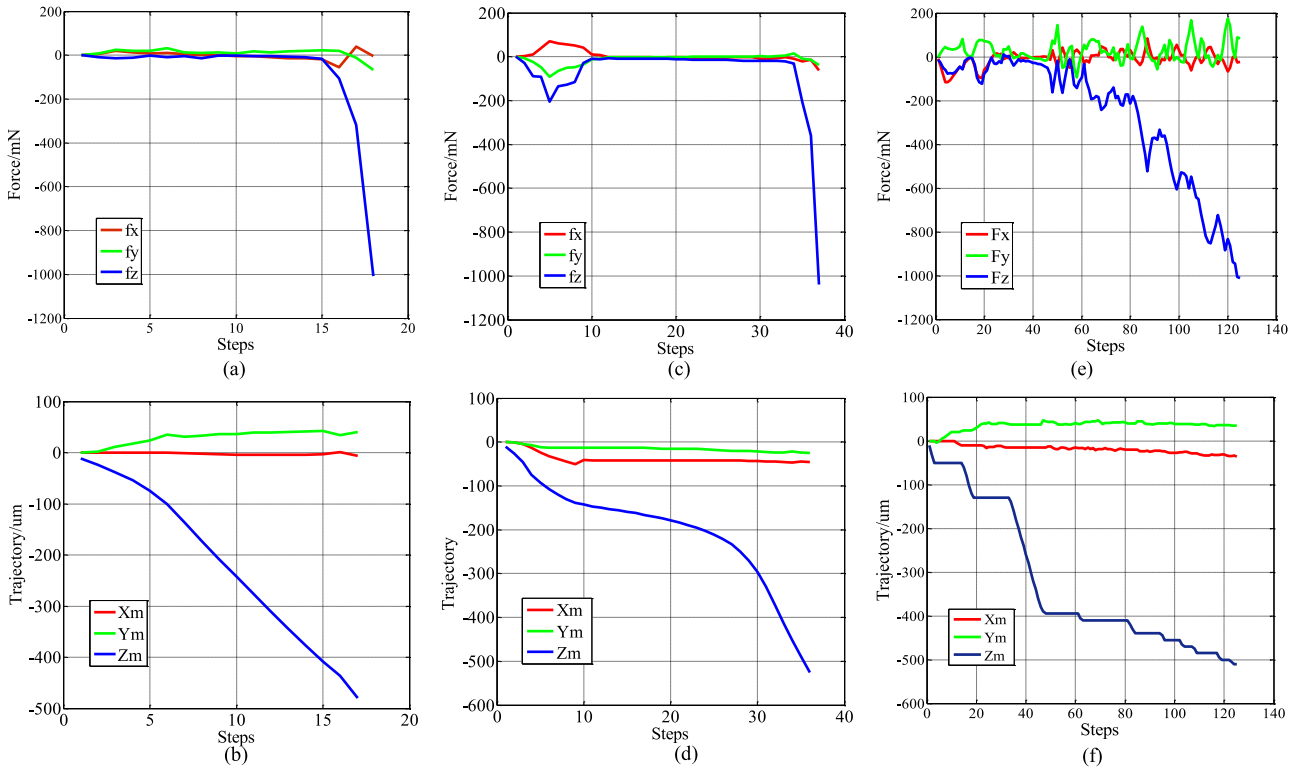

Fig. 8. Force curves and trajectories of insertion experiments. (a) Force curve without alignment error. (b) Trajectory without alignment error. (c) Force curve with alignment error. (d) Trajectory with alignment error. (e) Force curve of comparative experiment. (f) Trajectory of comparative experiment.

In this case, the state transition function will definitely performs in highest efficiency in dealing with the insertion task of the test components. However, it will loss generality in dealing with the assembly of other components.

Fig. 6 showed the tracking results of the matrix $\boldsymbol{J}$ to the force trajectories on testing dataset. The results showed that the lineal model captured most of the force variations, and the tracking errors can be described by the state transition function.

C. Insertion Experiments

Insertion experiments were designed to verify the feasibility and effectiveness of the proposed insertion control strategy, including insertion experiments with and without position alignment errors and comparative experiments with one of the existing insertion control methods. First of all, the global parameters of the insertion experiments, such as the $\Delta \boldsymbol{s}$, T_s, and the reward function, were set according to the Σ matrix.

The values of the reward function were assigned by Table I, which was l_2-form of the offset vector formed by the f_x and f_y of the state $\boldsymbol{s_{k+1}}$ versus the insertion depth of the action $\boldsymbol{a}_{k+1}$. The principle of setting the reward values was that building up confidence on the state transition function takes time, however, once the state transition function disappointed the strategy, the confidence dropped dramatically. The interval of 15 mN was set according to the standard deviation of the estimation error of f_x and f_y in Σ matrix, while the upper bound was set according to the mechanical property of the component B.

Based on the property of Gaussian distribution, the $\Delta \boldsymbol{s}$ was set as $[30, 30, 56]^{\mathrm{T}}$ mN, which was two times larger than the standard deviation of the estimation error of f_x and f_y in Σ matrix, while the parameter T_s was set as 0.68. Then, based on (25), the estimation depth N for the nth action estimation approach was 4. Finally, the threshold F_Z in the $\boldsymbol{s}_K$ was set as 1000 mN. The initial value for the parameters of Δf_{z1} and γ was set -20 mN and 0.2, respectively. The thresholds F_1 and F_2 for bounding Δf_{z1} were set to be 5 and 50 mN, respectively. The thresholds γ_1 and γ_2 for bounding γ were set to be 0.1 and 0.4.

The preparatory work of pose alignment was realized based on the microscopic vision system, with the orientation error less than 0.1° around $\boldsymbol{x_w}$- and $\boldsymbol{y_w}$- axis and the position error less than 2 μm along $\boldsymbol{x_m}$- and $\boldsymbol{y_m}$-axis. Insertion experiments without position alignment errors were first conducted. Detailed experiment results in one insertion task were given in Table II, in which R was the corresponding reward.

As shown in Table II, there were 17 steps involved in the insertion task to transit the state from $\boldsymbol{s}_0$ to $\boldsymbol{s}_K$. The end state was $[-4\ -68\ -1008]^T\ mN$. The assembled component was shown in Fig. 7. Fig. 8(a) and (b) showed the force curve and trajectory of this insertion experiment. The results demonstrate that the insertion process proceeded fluently, while the forces along $\boldsymbol{x_f}\ \boldsymbol{y_f}$ plane were tightly bounded around zero. This was exactly the expected behavior for the proposed controller.

Insertion experiment with alignment error was also conducted. The component **B** was moved 20 μm along $\boldsymbol{x_m}$-axis

TABLE III
COMPARATIVE EXPERIMENT RESULTS IN TEN EXPERIMENTS

Our Method				Method in [9]			
No.	Steps	No.	Steps	No.	Steps	No.	Steps
1	21	6	26	1	132	6	129
2	31	7	20	2	137	7	151
3	19	8	18	3	129	8	142
4	22	9	22	4	146	9	147
5	22	10	23	5	125	10	133

after alignment. Fig. 8(c) and (d) showed the force curve and movement trajectory of this experiment. The insertion process lasted for 36 steps. The larger force variation in the force curve aroused from overcoming the alignment error. After overcoming the alignment error, the insertion process lasted for another 25 steps which was more than the insertion steps of the experiment without alignment error. This phenomenon coincides with the principle of value assignment to the reward function.

D. Comparative and Repeatability Experiments

To verify the effectiveness and advantages of the proposed insertion method against the existing insertion control methods, comparative experiments were well conducted. The insertion method in [9] used a plain logic to control the insertion process, in which the components were inserted with fixed insertion depth and the modification of horizontal forces were always conducted to get ready for the insertion step. The insertion method in [9] was similar to the one in [8], with the difference that horizontal forces were modified with a scalar matrix instead of using the minimum movement resolution.

The parameters for the comparative experiment were set as follows: the threshold for horizontal force modification was 60 mN; the fixed insertion depth was 8 μm; the threshold for the end of the insertion was 1000 mN, and the scalar matrix for horizontal force modification was calibrated and given in

$$\begin{bmatrix} \Delta X_m \\ \Delta Y_m \end{bmatrix} = \begin{bmatrix} -0.24 & -0.25 \\ 0.04 & -0.07 \end{bmatrix} \begin{bmatrix} f_x \\ f_y \end{bmatrix}. \tag{29}$$

Fig. 8(e) and (f) showed the force curve and trajectories of the comparative method in one insertion task. The insertion process lasted for 125 steps. Compared with Fig. 8(a) and (c), the f_x and f_y force curve in Fig. 8(e) vibrated fiercely and the f_z force curve was stair stepping. It could be seen that from the 60th step on, most of the steps were for horizontal force modification while the inserted depth was only promoted for 100 μm.

Totally ten times experiments of both the proposed method and the method in [9] were conducted with the insertion steps listed in Table III. Table III shows that with the proposed method, the insertion could be finished in 20 to 30 steps. The efficiency of the proposed method was at least four times better than the method in [9]. Combining with the comparison results of the force curves and trajectories in Fig. 8, it was concluded that the proposed insertion control strategy can efficiently realize the insertion of cylindrical components with interference fit, while the force variation and the trajectory of the component during the insertion process behaves in expected manner.

TABLE IV
REPEATABILITY EXPERIMENT RESULTS ON FIVE COMPONENTS

Comp. No.	Exp. No.	Our Method [Steps]	Method in [9] [Steps]
1	1	29	138
	2	24	143
2	3	35	124
	4	42	136
3	5	33	142
	6	27	151
4	7	22	121
	8	24	137
5	9	31	131
	10	29	145

Additional experiments were conducted on other five different groups of components, twice experiments per group, as shown in Table IV. Most insertion tasks were finished with about 30 steps with the proposed method, while the insertion tasks based on the method in [9] needs at least 120 steps, which demonstrated the repeatability and generality of the proposed insertion control strategy.

VI. CONCLUSION

This paper reported our work on the development of an efficient insertion control strategy for cylindrical components with interference fit. The insertion of components is modeled as a stochastic state transition process with the uncertainty described by the Gaussian distribution. The state transition function is well defined based on the analysis of historical assembly data and the universal mechanical properties of the components. An assessment function is also elaborately designed to assess the performance of the state transition function. Finally, the action to be taken for the current state is decided by iterative calculations in N steps estimation manner. An automatic assembly system is developed to verify the effectiveness of the proposed control method. With the developed method, the insertion efficiency is significantly improved for the assembly tasks.

REFERENCES

[1] S. Liu, D. Xu, Y. F. Li, F. Shen, and D. Zhang, "Nano liter fluid dispensing based on microscopic vision and laser range sensor," *IEEE Trans. Ind. Electron.*, vol. 64, no. 2, pp. 1292–1302, Feb. 2017.
[2] J. Fluitman, "Microsystems technology: Objectives," *Sens. Actuators A, Phys.*, vol. 56, pp. 151–166, 1996.
[3] J. Zhang, D. Xu, Z. T. Zhang, and W. S. Zhang, "Position/force hybrid control system for high precision alignment of small gripper to ring object," *Int. J. Autom. Comput.*, vol. 10, no. 4, pp. 360–367, 2013.
[4] H. V. Brussel *et al.*, "Assembly of microsystems," *CIRP Ann., Manuf. Technol.*, vol. 49, no. 2, pp. 451–472, 2000.
[5] J. A. Franklin and H. Benbrahim, "Acquiring robot skills via reinforcement learning," *IEEE Control Syst. mag.*, vol. 14, no. 1, pp. 13–24, Feb. 1994.
[6] S. Liu, D. Xu, F. Liu, D. Zhang, and Z. Zhang, "Relative pose estimation for alignment of long cylindrical components based on microscopic vision," *IEEE/ASME Trans. Mechatronics*, vol. 21, no. 3, pp. 1388–1398, Jun. 2016.
[7] F. Shen, W. Wu, D. Yu, D. Xu, and Z. Cao, "High precision automated 3-D assembly with attitude adjustment performed by LMTI and vision based control," *IEEE/ASME Trans. Mechatronics*, vol. 20, no. 4, pp. 1777–1789, Aug. 2015.

[8] S. Liu, D. Xu, D. Zhang, and Z. Zhang, "High precision automatic assembly based on microscopic vision and force information," *IEEE Trans. Autom. Sci. Eng.*, vol. 13, no. 1, pp. 382–393, Jan. 2016.
[9] D. Xing, F. Liu, F. Qin, and D. Xu, "Coordinated insertion control for inclined precision assembly," *IEEE Trans. Ind. Electron.*, vol. 63, no. 5, pp. 2990–2999, May 2016.
[10] L. Ren, L. Wang, J. K. Mills, and D. Sun, "Vision-based 2-D automatic micrograsping using coarse-to-fine grasping strategy," *IEEE Trans. Ind. Electron.*, vol. 55, no. 9, pp. 3324–3331, Sep. 2008.
[11] S. Huang and J. M. Schimmels, "Admittance selection conditions for frictionless force-guided assembly of polyhedral parts in two single-point principal contacts," *IEEE Trans. Robot.*, vol. 24, no. 2, pp. 461–468, Apr. 2008.
[12] S. C. Wiemer and J. M. Schimmels, "Optimal admittance characteristics for planar force-assembly of convex polygonal parts," in *Proc. IEEE Int. Conf. Robot. Autom.*, 2012, pp. 2578–2583.
[13] K. Rabenorosoa, C. Clevy, and P. Lutz, "Active force control for robotic micro-assembly: Application to guiding tasks," in *Proc. IEEE Int. Conf. Robot. Autom.*, 2010, pp. 2137–2142.
[14] Q. Xu, "Robust impedance control of a compliant microgripper for high speed position/force regulation," *IEEE Trans. Ind. Electron.*, vol. 62, no. 3, pp. 1201–1209, Feb. 2015.
[15] D. Xing, D. Xu, and F. Liu, "Precision assembly among multiple thin objects with various fit types," *IEEE/ASME Trans. Mechatronics*, vol. 21, no. 1, pp. 364–378, Feb. 2016.
[16] W. Najy, H. Zeineldin, and W. Woon, "Optimal protection coordination for microgrids with grid-connected and islanded capability," *IEEE Trans. Ind. Electron.*, vol. 60, no. 4, pp. 1668–1677, Apr. 2013.
[17] T. Tang, H. Lin, Y. Zhao, Y. Fan, W. Chen, and M. Tomizuka, "Teach industrial robots peg-hole-insertion by human demonstration," in *Proc. IEEE Int. Conf. Adv. Intell. Mechatron.*, Jul. 12–15, 2016, pp. 488–494.
[18] I. F. Jasim and P. W. Plapper, "Contact-state recognition of compliant motion robots using expectation maximization-based Gaussian mixtures," in *Proc. 41st Int. Symp. Robot.*, Jun. 2–3, 2014, pp. 56–63.
[19] I. F. Jasim, P. W. Plapper, and H. Voos, "Position identification in force-guided robotic peg-in-hole assembly tasks," *Procedia CIRP*, vol. 23, pp. 217–222, 2014.

Song Liu received the B.Sc. degree in sensing technology and instrumentation from Shandong University, Jinan, China, in 2012, and the Ph.D. degree in control science and engineering from the Institute of Automation, Chinese Academy of Sciences, Beijing China; University of the Chinese Academy of Sciences, Beijing China; and Department of Mechanical and Biomedical Engineering, City University of Hong Kong, Kowloon, Hong Kong, in 2017.

His current research interests include visual measurement, visual servo control, micro-assembly, and micromanipulation.

You-Fu Li (SM'01) received the B.S. and M.S. degrees in electrical engineering from Harbin Institute of Technology, Harbin, China, and the Ph.D. degree in robotics from the Department of Engineering Science, University of Oxford, Oxford, U.K., in 1993.

From 1993 to 1995, he was Research Staff in the Department of Computer Science, University of Wales, Aberystwyth, U.K. In 1995, he joined the City University of Hong Kong, Kowloon, Hong Kong, where he is currently a Professor in the Department of Mechanical and Biomedical Engineering. His research interests include robot sensing, robot vision, and visual tracking.

Prof. Li has served as an Associate Editor for the IEEE TRANSACTIONS ON AUTOMATION SCIENCE AND ENGINEERING, an Associate Editor for the *IEEE Robotics and Automation Magazine* (RAM), an Editor for the Conference Editorial Board of the IEEE International Conference on Robotics and Automation, and a Guest Editor for the IEEE RAM.

Deng-Peng Xing received the B.S. degree in mechanical electronics and the M.S. degree in mechanical manufacturing and automation from Tianjin University, Tianjin, China, in 2002 and 2006, respectively, and the Ph.D. degree in control science and engineering from Shanghai Jiao Tong University, Shanghai, China, in 2010.

He is currently an Associate Professor with the Research Center of Precision Sensing and Control, Institute of Automation, Chinese Academy of Sciences, Beijing, China. His research interests include robot control and learning, precision assembly, and optimization.

De Xu (M'05–SM'09) received the B.Sc. and M.Sc. degrees from Shandong University of Technology, Jinan, China, in 1985 and 1990, respectively, and the Ph.D. degree from Zhejiang University, Hangzhou, China, in 2001, all in control science and engineering.

Since 2001, he has been with the Institute of Automation, Chinese Academy of Sciences (IA-CAS), Beijing, China. He is currently a Professor with the Research Center of Precision Sensing and Control, IA-CAS, and the University of the Chinese Academy of Sciences. His current research interests include robotics and automation, such as visual measurement, visual control, intelligent control, microscopic vision, and microassembly.

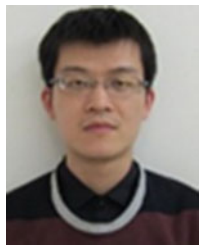

Hu Su received the B.Sc. degree in information and computing science and the M.Sc. degree in operational research and cybernetics from Shandong University, Jinan, China, in 2007 and 2010, respectively, and the Ph.D. degree in control science and engineering from the State Key Laboratory of Management and Control for Complex Systems, Institute of Automation, Chinese Academy of Sciences (IA-CAS), Beijing, China, in 2013.

Since 2013, he has been with the IA-CAS, where he is currently an Assistant Professor with the Research Center of Precision Sensing and Control. His current research interests include intelligent control and optimization and pattern recognition.